Crystal Structures of Optically Active Polyamides Derived from Di-*O*-methyl-L-tartaric Acid and 1,*n*-Alkanediamines: A Study Combining Energy Calculations, Diffraction Analysis, and Modeling Simulations

I. Iribarren, C. Alemán, J. J. Bou, and S. Muñoz-Guerra*

Departament d'Enginyeria Química, Universitat Politècnica de Catalunya ETSEIB, Diagonal 647, 08028 Barcelona, Spain

Received September 15, 1995; Revised Manuscript Received February 2, 1996[⊗]

ABSTRACT: The crystal structures of a series of optically active polyamides derived from L-tartaric acid and 1,*n*-alkanediamines (n = 2, 4, 6, and 8) have been investigated. Experimental data provided by X-ray diffraction of powders and fibers as well as by electron diffraction of single crystals were used to determine the lattice parameters for each polymer. A triclinic unit cell with space group *P*1 was found to be shared by the whole series. Semiempirical quantum mechanical calculations revealed that the preferred conformation for these polytartaramides entailed the tartaric acid moiety in a *gauche* arrangement with the amide groups rotated out of the plane containing the *all-trans* polymethylene segment. Crystal models compatible with the crystallographic data were built and refined against X-ray diffraction intensities with the linked-atom least-squares (LALS) methodology. The favored structure appeared to consist of hydrogen-bonded pleated sheets packed with a stagger similar to that found in the α-form of nylon 66. Modeling performed with CERIUS, a program enabling on-line observation of the simulated X-ray and electron scattering as the molecular model is adjusted, led to substantially similar results.

Introduction

Carbohydrate-based polyamides, *i.e.*, polysaccharamides, are receiving both increasing academic and industrial attention because of the natural abundance of their feedstocks and because they are promising materials with novel technical possibilities.[1] Varying properties, such as hydrophilicity/hydrophobicity, biodegradability, and potential biocompatibility with other naturals, make these polyamides interesting for a number of currently demanding applications. Polyaldaramides are linear polysaccharamides produced from aldaric acids and aliphatic diamines. Although polyaldaramides began to be explored in the earlier 1960s[2] and were extensively investigated by Ogata *et al.* along the 1970s,[3−6] a renewed interest in them has emerged in these last few years.[7−10] Recently, we have reported on the synthesis and properties of polytartaramides, which are polyaldaramides deriving from the naturally occurring tartaric acid.[11−14] Among the different types of polytartaramides that have been investigated by us, those based on 2,3-di-*O*-methyl-l-tartaric acid and 1,*n*-alkanediamines, namely P*n*DMLT,

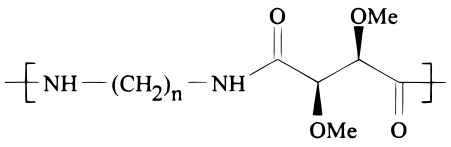

have been the object of preferential attention. They stand out by combining an overal desirable pattern of properties with relatively easy accessibility.

P*n*DMLT's are stereoregular polyamides that display high crystallinity and show large optical activity in solution. They exhibit a pronounced affinity for water and hydrolyze faster than conventional polyamides.[12] Melting points of the P*n*DMLT's fall within the interval 185−312 °C, with T_m describing a zigzag curve with local maxima and minima corresponding to polymers with even and odd values of *n*, respectively. By analogy with other series of polycondensation polymers consisting of flexible polymethylene segments of varying length,[15,16] such a correlation implies the existence of different crystalline structures in each case.

The crystal structures of polyaldaramides have not been investigated thus far, even though molecular arrangements departing from those typically adopted by conventional nylons may be expected for these highly substituted chiral polyamides. As with simple sugar derivatives,[17] repulsive effects between pendent oxy groups would be expected to prevent the backbone of the aldaric acid moiety to be in an extended conformation. Furthermore, possible intramolecular hydrogen bond interactions taking place between side-chain oxygen atoms and amide groups may contribute also to modify the conformation of the polymer. In this regard, several studies carried out on *N*-alkyl-D-gluconamides showed that these molecules crystallized in a sickle conformation arising from a change in the torsion angle around the C1−C2 bond in the alkyl chain and that the crystal lattice is stabilized by both inter- and intramolecular hydrogen bonds.[18,19] More recently, computer simulation studies based on experimental NMR data of polyaldaramides have been reported.[20] They suggest that certain hydroxyl unprotected polyaldaramides tend to form helical structures stabilized by intramolecular hydrogen bonds; the symmetry displayed by the helix seems to be determined largely by the stereochemical configuration of the carbohydrate moiety.[21]

As a first step in the development of a long-term project intended to investigate the conformations and crystal structures of polytartaramides in relation to their chemical constitution and properties, the present study has focused on P*n*DMLT's having even values of *n*. Powders, fibers, and single crystals of members with n = 2, 4, 6, and 8 were analyzed by X-ray diffraction and electron microscopy and the crystal structures

* To whom all correspondence should be addressed.
[⊗] Abstract published in *Advance ACS Abstracts,* May 1, 1996.

S0024-9297(95)01394-5 CCC: $12.00

Table 1. Characteristics of Polyamides P*n*DMLT Studied in this Work[a]

polyamide	M_w[b]	M_n[b]	T_m,[c] °C	T_g,[c] °C	$[\alpha]^{23}_D$[d]
P2DMLT	10 800	7 700	311.5		175.2
P4DMLT	25 100	15 200	266.1	100	121.0
P6DMLT	35 300	15 700	230.2	106	104.4
P8DMLT	69 300	44 600	208.1	89	92.4

[a] Data taken from ref 12. [b] Measured by GPC on trifluoroacetylated samples and calibrated against polystyrene standards. [c] Determined by DSC. [d] Measured in formic acid.

examined in light of the collected diffraction data. Due to the structural similitudes found for the different P*n*DMLT's, computational and modeling calculations were carried out basically on poly(hexamethylene-2,3-di-*O*-methyl-L-tartaramide) (P6DMLT) and the results obtained therefrom were extended to the other members of the series. The strategy adopted in this paper combines semiempirical quantum mechanical calculations with diffraction results to unravel the preferred conformations for the polytartaramide chain that are compatible with the crystallographic data. The energetically favored conformers were used to construct crystal models which were refined against X-ray data using the linked-atom least-squares (LALS) methodology.[22] A parallel modeling analysis has been performed by means of CERIUS,[23] a program enabling experimental diffraction patterns to be compared with those obtained from crystal models by computer simulation.

Materials and Methods

Experimental Procedures. The polytartaramides (P*n*DMLT, $n = 2, 4, 6, 8$) used in this work were prepared by polycondensation of bis(pentachlorophenyl) 2,3-di-*O*-methyl-L-tartarate with the corresponding 1,*n*-alkanediamines in a chloroform solution as described in detail elsewhere.[12] Some data of these polyamides relevant to the present study are given in Table 1.

Densities were measured at 25 °C on pieces of polymer films by the flotation method in a KBr 25% (w/w) aqueous solution. X-ray diffraction diagrams were recorded from both powders and fibers. Fibers of P6DMLT and P8DMLT were obtained by stretching the polymer from the melt and subsequent annealing at a temperature near the melting point. In order to avoid decomposition at heating, fibers of P4DMLT were prepared at room temperature by pulling out a concentrated solution of the polymer in formic acid. In contrast to the other members of the series, P2DMLT could not be oriented when the same methods were applied. X-ray diffraction diagrams were registered on flat films in a modified Statton-type camera using nickel-filtered Cu Kα radiation of wavelength 1.542 Å, and they were calibrated with molybdenum sulfide (d_{002} = 6.147 Å). Reflection maximum intensities were measured with a unidimensional Joyce Loebl MK III CS microdensitometer and corrected for polarization and Lorentz factors. In the case of fiber patterns, corrections taking into account the orientation of the diffracting planes were additionally made for every spot. However, no absorption correction was needed since the films used for diffraction were thin.

Electron microscopy observations were carried out on a Philips EM-301 instrument operating at 80 and 100 kV for bright field and electron diffraction, respectively. Crystallizations were accomplished isothermally from diluted solutions of polymers in either glycerol or triethylene glycol. Single crystals were recovered by centrifugation and, after repeated washing with 1-butanol, deposited on electron microscope carbon-coated grids. Crystals to be observed in the bright field were shadowed with Pt carbon at an angle of approximately 15°, whereas unshadowed samples were used for electron diffraction examination. Electron diffraction diagrams were recorded in the selected area mode under a minimum flux of radiation and were internally calibrated with gold (d_{111} = 2.35 Å).

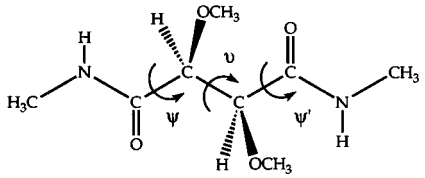

1

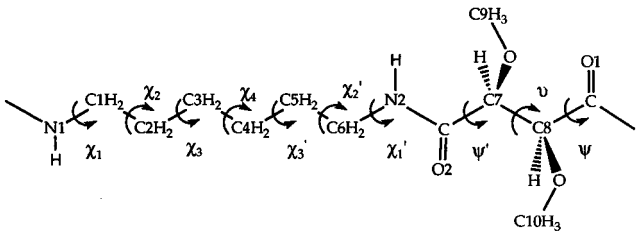

2

Figure 1. Chemical formulas of model compound *N,N'*-dimethyl-2,3-di-*O*-methyl-L-tartaramide (**1**) and the repeating unit of P6DMLT (**2**) with the dihedral angle and atom notations used in this work indicated.

Quantum Mechanical Calculations. *N,N'*-Dimethyl-2,3-di-*O*-methyl-L-tartaramide (**1**) was selected as the model molecule for calculating the conformational preferences of the tartaric unit in polyamides P*n*DMLT. Energy calculations were performed using the semiempirical AM1 Hamiltonian[24] which has been proved to be useful in the structural analysis of related polyamides.[25,26] Two specific cases were considered in these calculations: (*i*) $\Psi = \Psi'$ and (*ii*) $\Psi = -\Psi'$. In both cases, conformational maps for combinations of the dihedral angles Ψ and *v* were generated using the standard parameters implemented in the MOPAC package.[27] Potential energy surfaces were calculated using a grid of 20°. Torsional angles of the amide groups were held fixed at 180°, whereas all other geometrical parameters were relaxed. Then, the effect of internal rotations of the tartaric unit on an infinite polymer chain was analyzed. The repeating unit of P6DMLT (**2**) was used for these calculations, where contour conditions were applied in order to generate regular conformations. The chemical formulas of **1** and **2** with indication of the notations used to specify the conformational angles and atoms are represented in Figure 1. All the calculations were performed on an IBM/3090 computer at the Centre de Supercomputació de Catalunya (CESCA).

Crystal Model Building and Refinement. Those conformations of the tartaric unit favored by AM1 calculations were used for building the asymmetric unit of the P6DMLT chain by means of LALS. Bond lengths and angles were kept fixed at their standard values, and the amide group was held in a *trans* conformation. Standard hydrogen bond parameters were introduced and forced to be mantained within reasonable ranges of variations. The resulting models were then adjusted by taking into account both packing and geometric restrictions imposed by experimental diffraction data. Finally, the crystal structure was refined against X-ray intensities measured on fiber patterns.

The repeating unit of P6DMLT (**2**) in its energetically favored conformations was also used to model the crystal lattice of this polymer by CERIUS. The unit cell parameters and symmetry determined initially by X-ray and electron diffraction were used for generating the structure. Adjustments were made to satisfy contour conditions, namely, coincidence in the space at both ends of **2**. Forbidden close contacts between neighboring chains were removed, and hydrogen bonds were made between chains separated by appropriate distances. X-ray and electron diffractograms were simulated on-line and compared with those available from experiments. At this stage, the model was refined until optimum agreement between calculated and experimental data was attained. All CERIUS calculations and simulations were performed on a Silicon Graphics RI-4000.

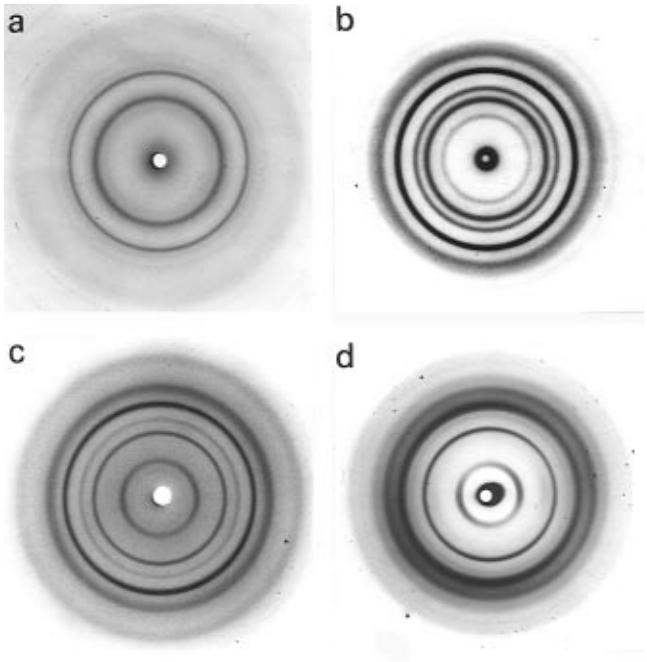

Figure 2. X-ray powder diffraction patterns of polytartaramides. (a) P2DMLT; (b) P4DMLT; (c) P6DMLT; (d) P8DMLT.

Results and Discussion

X-ray Diffraction. The powder diagrams recorded from P*n*DMLT for $n = 2$, 4, 6, and 8 are shown in Figure 2. The general appearance displayed by these patterns indicates that a notable crystallinity is present in all cases. When these diagrams are compared in detail, the possibility that a similar type of crystal structure is shared by the four polymers is immediately suggested. This was definitely confirmed by the results obtained in the diffraction analysis of oriented samples. The pattern shown in Figure 3a was taken from a fiber of P6DMLT stretched from the melt. Similar patterns were obtained from P4DMLT and P8DMLT. The dominant features common to the fiber diagrams of P*n*DMLT are (a) the existence on the equator of two strong reflections spaced at about 5.6 and 4.5 Å, respectively, and (b) the presence of an intense first layer line with a spacing steadily increasing with *n*, the latter obviously corresponding to the axial repeat of the structure. The similitude observed in the scattering along the equator demonstrates that the same side-by-side packing of chains is adopted in all cases. On the other hand, the distribution of the reflections along the strata reveals that the 00*l* planes are inclined about 60° with respect to the polymer chains, which are aligned parallel to the fiber axis.

A triclinic lattice containing one chain per unit cell was found to be consistent with the diffraction data available for the four polymers. According to what is usual in nylons,[28] the structure is interpreted as a stacking of hydrogen-bonded sheets regularly staggered. The interchain distance within the sheets is about 5 Å, which coincides with the *a* dimension of the crystal; the intersheet distance is given by the 010 spacing and ranges from 5 to 6 Å. Indexing of the four polymers on the basis of this structure together with their respective observed and calculated spacings is listed in Table 2.

The *c* dimension of the structure, *i.e.*, the axial repeat length, was found to vary from 10.8 to 15.7 Å as *n* increased from 4 to 8. This implies that polytartaramides P*n*DMLT with $n = 4$, 6, and 8 crystallize with the chain contracted about 1.5−2 Å per repeating unit

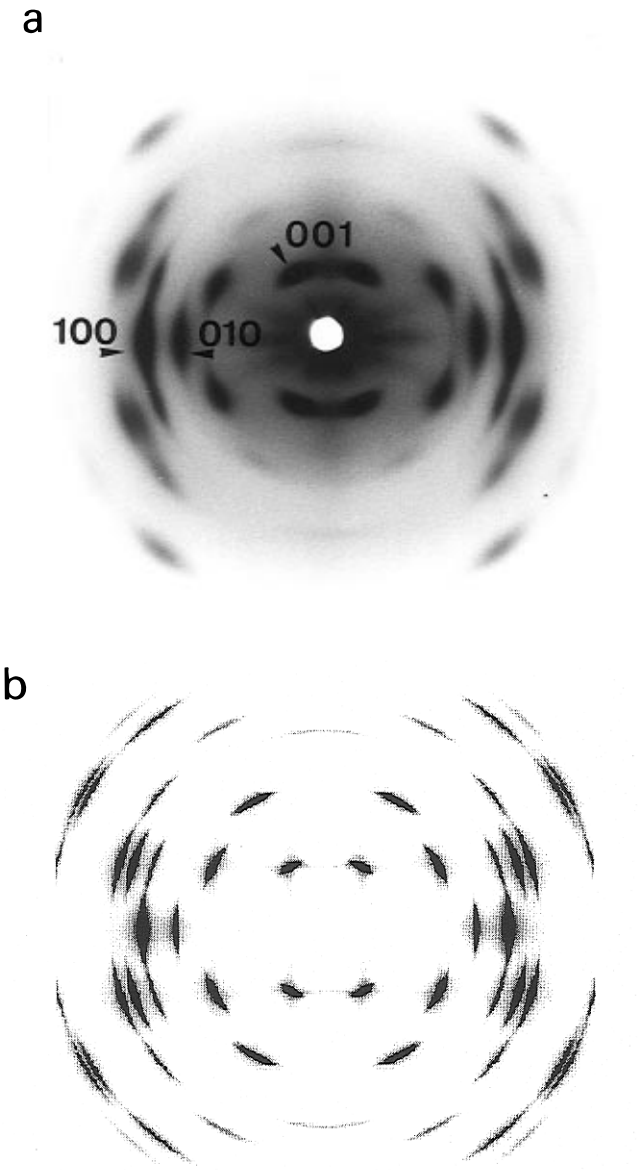

Figure 3. X-ray fiber diffraction patterns of P6DMLT. The fiber axis is vertical. (a) Experimentally observed pattern. (b) Pattern simulated by CERIUS from the triclinic model P1.

with respect to the *all-trans* conformation adopted in the α-form of nylons.[28] The puckering is still considerably deeper than that taking place in the γ-form of nylons.[15] The plot of *c* against *n* results in a straight line (Figure 4) with a slope of about 1.20 Å, which is a distance slightly shorter than the calculated mean rise of one methylene in the *trans* conformation (1.26 Å). Such a small but significant difference could be accounted for if the polymethylene segment is assumed to be tilted about 20° with respect to the *c* axis. On the other hand, when *n* is made to be equal to 0, a value close to 6 Å is inferred for *c*, which represents the height of the sequence $-HNCOCH(OCH_3)CH(OCH_3)CONH-$ in the three polytartaramides. In order to be accommodated in such a space, the tartaric moiety must assume a skewed conformation provided that the −HNCO− groups retain their usual planar arrangement.

A rather different situation is thought to occur in the case of P2DMLT, where the shortening of the axial repeat turns out to be less than 1 Å per residue. Although diffraction data obtained from this compound are comparatively poor, the deviation observed for the

Table 2. Interplanar Spacings (d_{hkl}) and Crystal Lattice Parameters (Å) of Polyamides P*n*DMLT

			P2DMLT		P4DMLT			P6DMLT			P8DMLT		
			d(obsd)		*d*(obsd)			*d*(obsd)			*d*(obsd)		
h	*k*	*l*	X-rays	*d*(calcd)	X-rays	ED	*d*(calcd)	X-rays	ED	*d*(calcd)	X-rays	ED	*d*(calcd)
0	1	0	5.60	5.55	5.60	5.65	5.58	5.53	5.45	5.46	5.18		5.15
1	0	0	4.65	4.67	4.60	4.60	4.59	4.57	4.60	4.54	4.54	4.60	4.51
−2	1	0	2.50	2.50	2.50		2.50	2.50	2.50	2.50	2.50	2.50	2.50
0	0	1	7.65	7.67	9.03		9.08	11.20		11.33	12.60		12.74
0	1	1	6.43	6.43	6.62		6.64	6.40	6.35	6.35	6.18	6.20	6.20
1	0	1	4.32	4.35	4.53		4.50	4.60		4.57	4.65		4.63
0	−1	1			3.89		3.90	4.17		4.15	3.97		4.03
1	1	1			3.30		3.31	3.20	3.19	3.20	3.10	3.15	3.11
0	1	2								5.63	6.10		6.12
1	0	2	4.48	4.48	3.60		3.65	4.00		3.98	4.23		4.22
0	2	2							3.15	3.18		3.05	3.10
1	0	3			2.83		2.82	3.26		3.27	3.58		3.57
0	1	4			2.68		2.67	3.30		3.30	3.93		3.92
1	0	4						2.69		2.67	2.99		2.98
0	1	5						2.63		2.62	3.12		3.12
0	1	6						2.18		2.16	2.54		2.56
a, *b*, *c*			4.95, 6.87, 9.10		5.00, 7.06, 10.80			5.00, 6.84, 13.20			5.00, 6.82, 15.7		
α, β, γ			59.0, 90.0, 106.6		59.4, 90.0, 110.0			61.5, 90.0, 111.6			57.0, 90.0, 111.3		
ρ, g mL^{-1}													
obsd				1.25			1.21			1.13			1.18
calcd				1.34			1.26			1.19			1.18

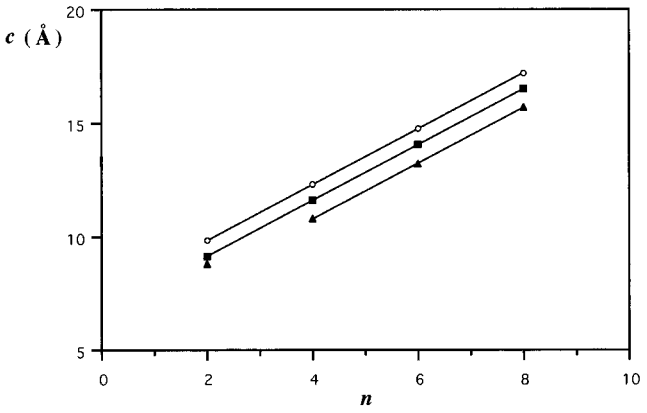

Figure 4. Repeating unit length of polyamides *n*,4 plotted against *n* for different conformations. ○, fully extended conformation characteristic of the α-form; ■, 2_1 helical conformation characteristic of the γ-form; ▲, conformation observed for the polytartaramides studied in this work.

value of *c* is out of the acceptable margin of experimental error. Accordingly, the conformation of the chain in P2DMLT is thought to be more relaxed than in other P*n*DMLT's in spite of the fact that the same type of crystal lattice seems to be adopted by this polymer.

Electron Microscopy and Electron Diffraction. Crystallization of polyamides P*n*DMLT for $n = 4$, 6, and 8 from diluted solutions in polyols yielded lamellar crystals of the type shown in Figure 5. Attempts made to crystallize P2DMLT under similar conditions were unsuccessful. The morphological features displayed by the crystals are those typical of polymers crystallizing in a lattice comprised of chains interlinked by a unidirectional array of hydrogen bonds.[29] They have in common a thickness of about 60 Å, which is within the 40−80-Å range usually observed for polyamide lamellae with chains arranged in a layered structure.[30] Furthermore, their width-to-length ratio tends to increase with the value of *n*, as reasonably expected for a gradual decreasing in hydrogen-bonding density.

The electron diffraction patterns recorded from these crystals were consistent with the triclinic structure established on the sole basis of X-ray data. Moreover, their great similarities corroborate the occurrence of a common side-by-side mode of packing for all the P*n*DMLT's and imply that the hydrogen-bonded sheets run parallel to the long dimension of the crystals. Due to the oblique geometry of the triclinic lattice, diffraction patterns composed of *hkl* reflections with $l \neq 0$ were registered more frequently than those corresponding to the [001] axis zone. In addition, some reflections may appear occasionally doubled, in particular those arising from 0*kl* planes. The few number of repeating units accommodated within the lamellar height entails a distortion of the reciprocal lattice, meaning that more than one plane may be intercepted by the Ewald sphere. These features become well illustrated in the diagram depicted in Figure 6a, which was recorded from a crystal of P6DMLT lying on its basal plane, *i.e.*, with the chains leaning about 30° with respect to the electron beam direction. The spacings measured for each polymer by electron diffraction, regardless of which was the diffracting zone recorded, are compiled in Table 2 where they can be compared with those estimated by X-ray diffraction.

Conformational Analysis of the Tartaric Acid Unit. The Ψ−*v* conformational energy maps resulting for model compound **1** under the constraints stated for cases *i* and *ii* are shown in Figure 7. Contour lines are drawn for energy increments of 1 kcal mol^{-1}, revealing that several low-energy conformational regions (below 5 kcal mol^{-1}) are possible for both cases. Whereas low-energy regions appear clearly separated in case *i*, contour lines from 3 kcal mol^{-1} upwards enveloping a continuous range of favored conformations are found for case *ii*. In the latter case, the map becomes symmetrical with respect to the line $\Psi = 180°$, as expected from the conformational analogy resulting for opposite values of Ψ and Ψ′. Relative energies and dihedral angles calculated for the minimum-energy conformations existing in the low-energy regions found in each case are listed in Table 3.

The low-energy conformations computed in the gas-phase for model compound **1** should be considered only as a first approximation to initiate the polymer structure simulation. Since the crystal field may modify the relative energy order resulting from such calculations, all the conformations included in Table 3 were initially taken into account for the construction of the polymer chain.

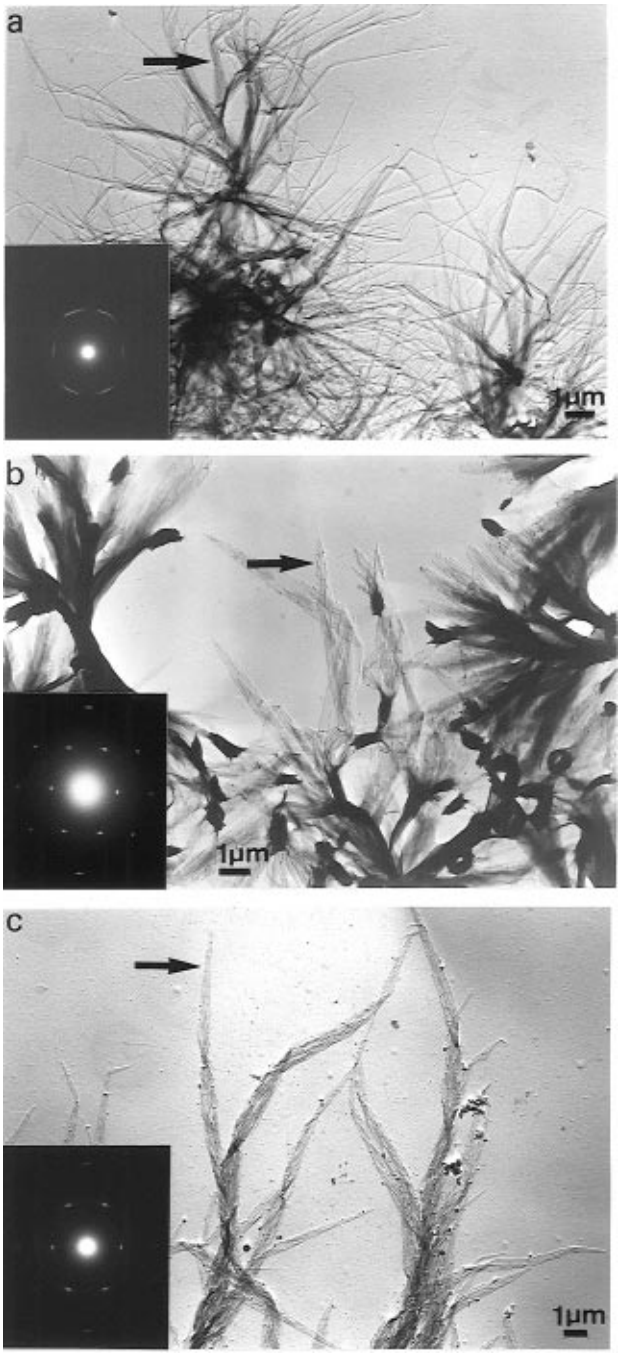

Figure 5. Lamellar crystals of P*n*DMLT isothermally grown from solution and their corresponding electron diffraction patterns. (a) P4DMLT; (b) P6DMLT; (c) P8DMLT. Arrows indicate the orientation of the crystal relative to the diffraction pattern.

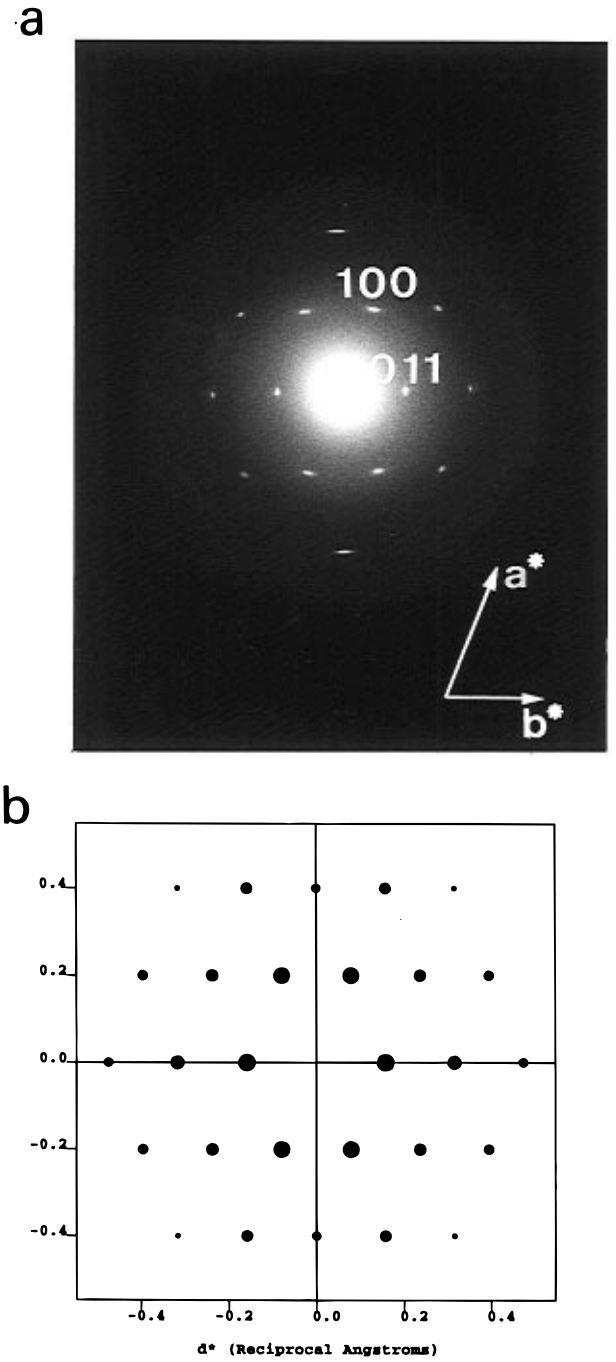

Figure 6. Single-crystal electron diffraction patterns of P6DMLT. (a) Experimentally observed pattern. (b) Electron diffraction pattern simulated for the [012] axis zone of the triclinic structure (P1 model).

Conformation of the Polytartaramide Chain. The conformational analysis and subsequent model building and simulations were carried out primarily for polyamide P6DMLT. In view of the structural analogies evidenced by diffraction experiments, the conclusions obtained therein may be reasonably extended to P4DMLT and P8DMLT.

In the first step, the values of the dihedral angles given for the seven favored conformations of **1** were used to build the repeating unit of P6DMLT, and the unit heights resulting for each case were compared with the experimental value of $c = 13.20$ Å determined by X-ray diffraction. In order to attain a satisfactory agreement between calculated and observed data, the dihedral angles χ_1 and χ_1' were varied, whereas all other dihedrals involved in the polymethylene segment (χ_2, χ_3, χ_4, χ_2', and χ_3') were frozen in an *all-trans* conformation. This approach takes after the γ-form of nylons where the C−N bond is known to be rotated, causing the polymethylene zigzag to abandon the plane of the amide group.[15] By this means, an additional contraction of around 0.35 Å per amide group is attained. Our results revealed that only the a and g low-energy conformations of the tartaric acid unit were able to provide a chain repeat compatible with the experimental data. The values resulting for the torsion angles about the N−C bonds in these two conformations were respectively $\chi_1 = \chi_1' = 85°$ and $\chi_1 = -\chi_1' = 101°$. The initial tartaric dihedrals were slightly modified also in order to achieve an optimum adjustment. The repeating unit of the two conformers are schematically represented in Figure 8, showing that the only remarkable difference between them is concerned with the relative

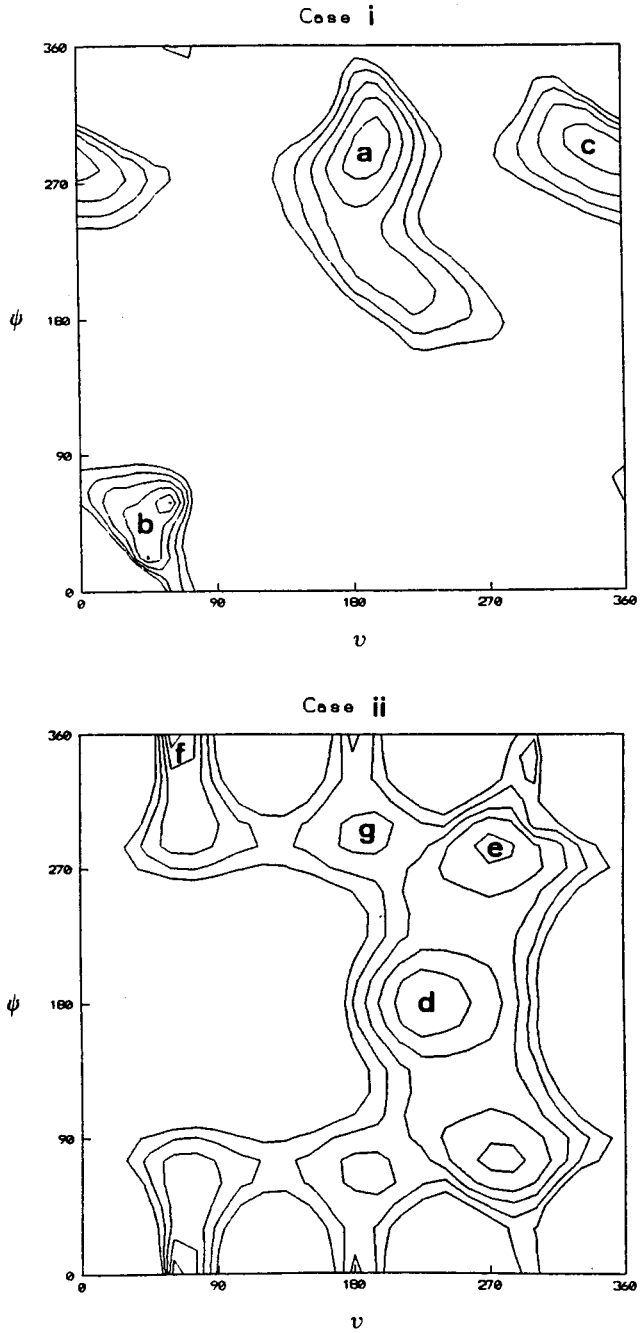

Figure 7. Conformational maps of model compound *N,N′*-dimethyl-di-*O*-methyl-L-tartaramide for cases (*i*) $\Psi = \Psi'$ and (*ii*) $\Psi = -\Psi'$.

Table 3. Torsional Angles (deg) and Relative Energies (kcal mol^{-1}) of the AM1 Low-Energy Conformations for Model Compound 1

case	model	Ψ	v	Ψ'	ΔE
i	**a**	−60	−160	−60	0.0
	b	60	40	60	1.3
	c	−80	0	−80	1.4
ii	**d**	180	−140	180	0.0
	e	−80	−80	80	0.5
	f	−20	60	20	1.2
	g	−60	180	60	2.3

orientation of the two amide groups contained in the asymmetric unit. In model a, the carbonyls are pointing in directions approximately 60° to each other, whereas they are arranged nearly in a *trans* conformation in the g model. The spatial arrangement adopted by the HNCO groups along the chain will play an important role in the formation of the hydrogen bonds and will

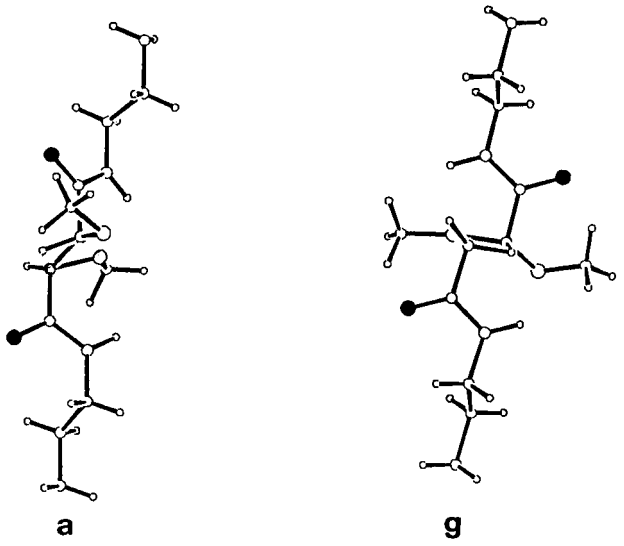

Figure 8. Schematic representation of the two conformations favored for the asymmetric unit of P6DMLT corresponding respectively to conformations **a** and **g** of the tartaric unit. Model **a**: $\Psi = \Psi' = -60°$; $\chi_1 = \chi_1' = 85°$. Model **g**: $\Psi = -\Psi' = -60°$; $\chi_1 = -\chi_1' = -101°$.

determine the degree of polarity displayed by the crystal structure.

A further interesting feature of these conformations which is worthy of comment concerns the *gauche* effect between lateral methoxy oxygens. It is known that glycols with the *threo* configuration tend to be arranged with the dihedral angle O−C−C−O near ±60° in order to relieve electronic interactions between neighboring oxygens.[31] The dihedral values calculated for such sequence in P6DMLT were −43.4° and −63.3° for models a and g, respectively. In both cases, the interaction between the vicinal OR groups becomes alleviated, in particular in model g, where the dihedral attains a value very near to that considered to be a standard *gauche* conformation. The same effect has been recently reported to occur in other related compounds, as is the case for certain cyclic acetals of L-tartaramides.[32]

Crystal Structure Modeling and Refinement by LALS. Crystal models were constructed with LALS by placing the repeating unit of P6DMLT (**2**) with the tartaric moiety in a or g conformation and the remaining part of the molecule in an arbitrary arrangement, into the experimentally determined unit cell. The overall conformation had to be slightly modified in order to bring the ends of the repeating unit into coincidence in the space. Space groups *C*2 and *P*1 were adopted for conformations a and g, respectively, in agreement with their respective molecular symmetries. In the former case, the unit cell was monoclinic and contained two chains related by 2-fold rotation and screw axes, whereas in the second case, the unit cell was triclinic. Although both conformations appeared to be feasible on stereochemical grounds, they showed notable differences in their ability to form hydrogen bonds. The best hydrogen-bond geometry attained for the model with chains in conformation a involved a N−H···O angle smaller than 150° and a N···O distance larger than 3.3 Å. Such parameter values turn out to be quite unusual for hydrogen bonding in polyamides.[33] Furthermore, they are in clear disagreement with infrared data reported for polytartaramides,[12] which indicated that hydrogen-bonding interactions in these systems are not very different in strength to those taking place in conventional nylons. On the contrary, all hydrogen bonds could be comfortably made in the model made up of

Table 4. Observed and Calculated Spacings (d_{hkl}, in Å) and Structure Factors (F) for the P1 Model of P6DMLT

spot	h	k	l	d_{obsd}	F_{obsd}	d_{calcd}	F_{calcd}	$F_{obsd} - F_{calcd}$
				Equator				
1	0	1	0	5.53	11.48	5.46	10.89	0.59
2	1	0	0			4.54		
	−1	1	0	4.57	19.37	4.55	20.24	−0.87
3	1	1	0			2.95		
	−1	2	0		4.66	2.94	6.80	−2.14
4	0	2	0		3.48	2.73	3.85	−0.37
5	−2	1	0	2.50	0.89	2.50	1.76	−0.87
				First Layer Line				
6	0	0	1	11.20	37.07	11.33	42.54	−5.47
7	0	1	1	6.40	10.60	6.35	13.76	−3.16
8	1	0	1			4.57		
	−1	1	1	4.60	29.30	4.57	25.93	3.37
9	0	−1	1	4.17	19.49	4.15	21.43	−1.94
10	1	1	1			3.20		
	−1	2	1	3.20	14.28	3.19	13.02	1.26
11	1	−1	1			2.61		
	−1	−2	1		16.47	2.60	12.90	3.57
				Second Layer Line				
12	0	0	2			5.66		
	0	1	2	5.67	13.98	5.63	18.56	−4.58
13	1	0	2			3.98		
	−1	1	2	4.00	18.46	3.98	20.64	−2.18
14	0	2	2			3.18		
	2	0	2			3.18		
	0	−1	2			3.20		
	1	1	2			3.21		
	1	−1	2			3.22		
	−1	2	2	3.15	9.17	3.22	8.83	0.34
				Third Layer Line				
15	0	1	3			3.27		
	−1	1	3	3.26	11.45	3.27	12.15	−0.70
				Fourth Layer Line				
16	1	0	4	3.30	6.67	3.30	10.50	−3.83

chains in g conformation. These findings enabled us to discard the model based on conformation a (C2 model) and to consider the triclinic lattice in space group $P1$ as the preferred model (P1 model) for the crystal structure of P6DMLT.

The P1 model was refined against X-ray intensities measured on the fiber diffraction pattern shown in Figure 3a. Sixteen independent spots were used for refinement, leading to a satisfactory R factor of 14.5%. Observed and calculated spacings and structure factors for all the reflections used in the refinement process are compared in Table 4. When the C2 model was subjected to similar refinement, an R factor well out of acceptable limits was obtained. A comparative description of models C2 and P1, including conformational and crystal parameters as well as the geometry of the optimized hydrogen bonds, is given in Table 5. The Cartesian coordinates for all the atoms included in the asymmetric unit of P6DMLT in the P1 model are given in Table 6. The three projections (a, b, and c) of model P1 drawn by means of the ORTEP program[34] are depicted in Figure 9.

Features of the crystal structure of P6DMLT which are worth noting are as follows:

(1) The conformation of the molecule is certainly complex, with the tartaric unit arranged as *gauche*, the diamine unit twisted at the HN−CH_2 bond, and the polymethylene segment in the *all-trans* conformation; the result is a compressed chain describing a wavy trajectory which follows the c axis of the structure.

(2) Although the formal unit cell is triclinic because of the lack of symmetry of the molecule in the g conformation, the chains are positioned in a rectangular

Table 5. Unit Cell Parameters, Conformational Angles, and Hydrogen-Bond Geometries[a] for the P1 and C2 Crystal Models of P6DMLT

	LALS		CERIUS	
	P1	C2	P1	C2
unit cell parameters				
a	5.00	5.00	5.00	5.00
b	6.84	12.65	6.84	12.6
c	13.20	13.20	13.20	13.20
α	61.5	60.0	61.5	60.0
β	90.0	90.0	90.0	90.0
γ	111.6	90.0	111.6	90.0
torsional angles				
Ψ	−76.2	−86.5	−50.2	−80.0
υ	−179.0	177.0	180.0	180.0
Ψ'	76.2	−86.5	50.2	−80.0
χ_1	−131.7	110.3	−101.0	85.0
$\chi_2 = \chi_3 = \chi_4 = \chi_2' = \chi_3'$	180.0	180.0	180.0	180.0
c_1'	131.7	110.3	101.0	85.0
H-bond geometry				
d(H···O)	1.92	3.42	1.89	2.52
d(N···O)	2.93	3.77	2.90	3.29
∠N−H···O	173.8	102.5	170.0	146.6
R factor, %	14.5	>50		

[a] Distances in Å and angles in deg.

Table 6. Cartesian coordinates of one residue of model P1 of P6DMLT

atom	x	y	z
N1	−6.895	−7.851	−10.478
H−N1	−6.536	−7.619	−11.393
C1	−6.594	−7.210	−9.190
H1−C1	−7.125	−6.261	−9.123
H2−C1	−6.912	−7.862	−8.376
C2	−5.078	−6.959	−9.082
H1−C2	−4.758	−6.306	−9.895
H2−C2	−4.546	−7.908	−9.148
C3	−4.762	−6.288	−7.732
H1−C3	−5.081	−6.938	−6.918
H2−C3	−5.294	−5.337	−7.665
C4	−3.246	−6.035	−7.624
H1−C4	−2.927	−5.383	−8.437
H2−C4	−2.714	−6.984	−7.690
C5	−2.931	−5.363	−6.274
H1−C5	−3.249	−6.015	−5.460
H2−C5	−3.462	−4.413	−6.207
C6	−1.414	−5.111	−6.166
H1−C6	−1.095	−4.460	−6.979
H2−C6	−0.882	−6.060	−6.232
N2	−1.007	−4.470	−4.907
H−N2	−1.437	−4.843	−4.083
C═O2	−0.132	−3.468	−4.877
O2	0.391	−3.018	−5.908
C7	0.153	−2.947	−3.484
O−C7	0.272	−3.985	−2.630
H−C7	1.081	−2.374	−3.492
C8	−1.005	−2.039	−3.027
O−C8	−2.147	−2.758	−2.973
H−C8	−1.126	−1.219	−3.735
C9	0.527	−3.521	−1.388
H1−C9	0.625	−4.360	−0.699
H2−C9	1.455	−2.949	−1.396
H3−C9	−0.292	−2.879	−1.065
C10	−3.162	−1.963	−2.573
H1−C10	−4.083	−2.543	−2.530
H−C10	−2.940	−1.560	−1.585
H−C10	−3.282	−1.143	−3.281
C═O1	−7.758	−8.842	−10.268
O1	−8.189	−9.112	−9.137

array of 5.0 × 12.6 Å; this accounts for the orthogonality observed in the electron diffraction patterns.

(3) Hydrogen bonding takes place along the a direction of the crystal, giving rise to nonpolar sheets composed of chains spaced out 5.0 Å; this distance is significantly larger than that normally found in hydrogen-bonded sheets of polyamides[30] and polypeptides,[35] which used to be in the range 4.6−4.9 Å.

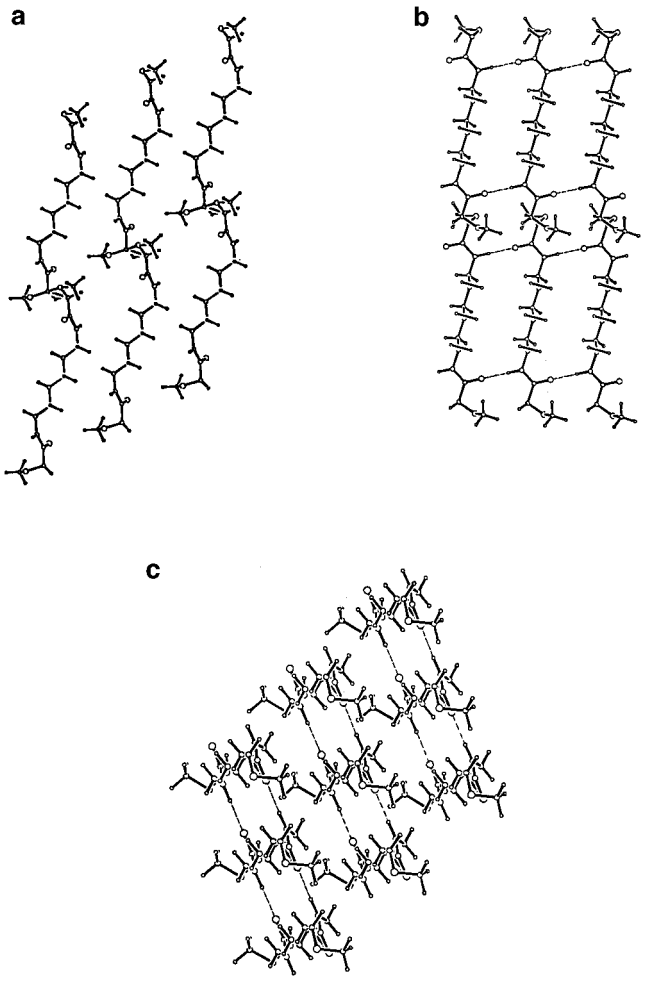

Figure 9. Views of the a, b, and c crystallographic planes of the triclinic structure (model P1) of polytartaramide P6DMLT.

(4) The tartaric units are located at the same level within the sheets, but they are regularly shifted along the *b* direction of the crystal. This enables the structure to save some room to accommodate the lateral methoxy groups in the intersheet space.

The conclusions drawn for P6DMLT may be readily extended to P4DMLT and P8DMLT provided that the corresponding enlargement of the axial repeat of the structure is duly taking into account. On the other hand, the discordant *c* value recorded for P2DMLT prevents us from doing the same in this case, although a similar structure is likely to be adopted by the polymer. Unfortunately, insufficient experimental data could be obtained for P2DMLT for a detailed analysis of its structure to be undertaken with acceptable reliability.

Modeling and Diffraction Simulation by CERIUS. CERIUS has been reported to be a useful tool in the structural study of polymers for which sufficient diffraction data are available and the conformation of the asymmetric unit in the gas-phase state has been previously established.[36,37] Since both conditions are fulfilled in the case of P6DMLT, it was considered of interest to see how crystal models of this polymer constructed by CERIUS compare to those generated by LALS. Furthermore, since CERIUS affords the possibility of simulating the diffraction patterns from a given crystal model, the program may be used to check the validity of the proposed structures.

Firstly, the asymmetric unit of polyamide P6DMLT in either conformation a or g was placed at the origin of the unit cell, and the symmetry operations implicit in space group *C*2 or *P*1 were applied accordingly. Stereochemical conclusions similar to those derived from the LALS analysis were drawn when contour conditions were imposed. The triclinic unit cell with the chain in the g conformation appeared to be the favored model also, and therefore, this was the structure primarily considered henceforth. The orientation and position of the chain within the lattice was then adjusted in order to obtain an optimum correspondence between calculated and experimentally observed diffraction patterns. The conformation of the chain was only slightly modified at this stage. Diffraction patterns with three different textures, powder, fiber, and single crystal, were used for this purpose.

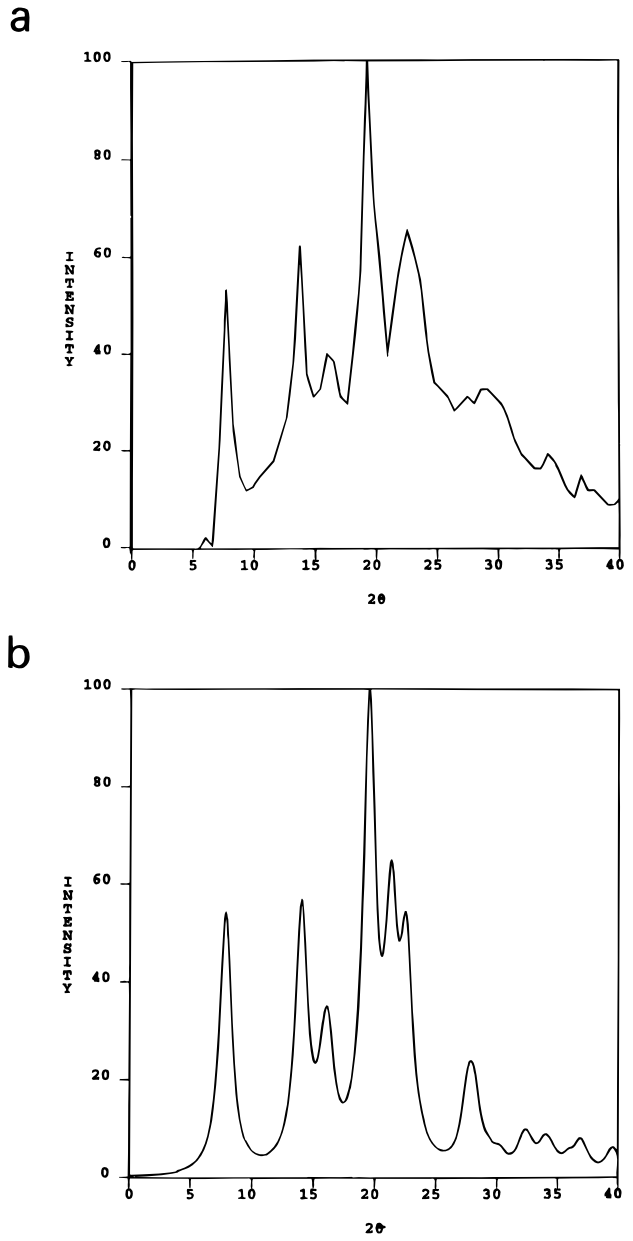

Figure 10. Compared profiles of experimental (a) and simulated (b) powder diffraction pattern of model P1 for polytartaramide P6DMLT.

(i) X-ray Powder Patterns. In Figure 10, the experimental X-ray powder diffraction pattern is compared with that simulated for the P1 model. The numerical intensities estimated for the six rings which appear clearly differentiated in the powder diagram of P6DMLT (shown in Figure 2c) are given in Table 7. A very good agreement was obtained for both positions and intensities of the maxima with a satisfactory *R*

Table 7. Simulation of the X-ray Powder Diagram of P6DMLT: Comparison between Observed[b] and Calculated Intensities for the P1 and C2 Crystal Models

						I_{calcd}	
ring	*h*	*k*	*l*[a]	d_{obsd}, Å	I_{obsd}	P1	C2
1	0	0	1	11.50	53	63	100
2	0	1	1	6.35	68	62	5
3	0	1	0	5.40	19	20	44
4	1	0	0				
	1	0	1	4.60	100	114	56
5	0	−1	1	4.17			
	1	0	2	3.95	92	101	9
6	−2	1	0	2.50	7	9	2

[a] Indexes taken from Table 2. [b] Spacings measured on the powder diagram shown in Figure 2c.

factor of 13.4%. A good concordance between calculated and observed diffraction powder diagrams is considered to be prerequisite for further consideration of the simulated structure. The agreement attained for the simulated diffraction pattern generated from the C2 model was much poorer. This was mainly due to the symmetry restraints imposed by space group *C*2, which limited severely the flexibility of the refinement procedure.

(ii) X-ray Fiber Patterns. The X-ray diffraction pattern of a fiber P6DMLT in the triclinic structure generated by CERIUS is shown in Figure 3b. The analogy achieved in both positions and intensities of the reflections is excellent. All the equatorial reflections and layer lines are satisfactorily reproduced. It should be noted that the appearance of the calculated fiber diagram appears to be highly sensitive to orientational effects. Therefore, much care must be taken in defining the orientation factor of the fiber in the simulation proccess in order to achieve reliable results.

(iii) Electron Diffraction Patterns. Electron diffraction patterns recorded from single crystals of P6DMLT contain reflections corresponding to more than one reciprocal plane. The diagram shown in Figure 6a is interpreted as arising from a crystal lying on the 001 crystal plane. In order to reproduce properly such a diagram, electron diffraction patterns were calculated by tilting the crystal around the *a*-axis. The simulated pattern arising from the [012] axis zone of the crystal (tilting conditions: $\theta \approx 30°$, $\varphi = 0°$) is shown in Figure 6b; the concordance with the experimental pattern is satisfactory for both distribution and intensities of diffraction maxima.

The conformational parameters and hydrogen-bond geometry calculated with CERIUS for the P1 model after adjustment and for the crude C2 model have been included in Table 5 to illustrate how they compare with those coming out from modeling by LALS. A reasonable agreement is found between the results obtained by the two methods, in particular when differences between models P1 and C2 are considered. It should be noted that the torsional angles resulting for the model refined by CERIUS are very close to those introduced in the starting conformations. This is mainly due to the fact that small changes in the dihedral angles hardly affect the appearance of the simulated diffraction patterns. This is one of the main reasons requiring that an energy conformational analysis has to be carried out prior to the modeling with CERIUS.

Acknowledgment. Financial support to carry out this study given by the CICYT (Comisión Interministerial de Ciencia y Tecnología, Grant No. MAT93-0555-CO2-02) is gratefully acknowledged. We are indebted to CESCA for computational facilities.

References and Notes

(1) Thiem, J.; Bachmann, F. *Trends Polym. Sci.* **1994**, *12*, 425.
(2) Bird, T. P.; Black, W. A. P.; Deward, E. T.; Hare, J. B. *J. Chem. Soc.* **1963**, 1208.
(3) Ogata, N.; Sanui, K.; Iijima, K. *J. Polym. Sci., Polym. Chem. Ed.* **1973**, *11*, 1095.
(4) Ogata, N.; Hosoda, Y. *J. Polym. Sci., Polym. Chem. Ed.* **1975**, *13*, 1973.
(5) Ogata, N.; Sanui, K. *J. Polym. Sci., Polym. Chem. Ed.* **1977**, *15*, 1523.
(6) Ogata, N.; Sanui, K.; Nakamura, H.; Kuwahara, M. *J. Polym. Sci., Polym. Chem. Ed.* **1980**, *18*, 939.
(7) Bachmann, F.; Thiem, J. *Makromol. Chem.* **1993**, *194*, 1035.
(8) Hashimoto, K.; Wibullucksanakul, S.; Matsuura, M.; Okada, M. *J. Polym. Sci., Polym. Chem. Ed.* **1993**, *31*, 3141.
(9) Kiely, D. E.; Chen, L.; Lin, T.-H. *J. Am. Chem. Soc.* **1994**, *116*, 571.
(10) Bueno, M.; Galbis, J. A.; García-Martín, M. G.; De Paz, M. V.; Zamora, F.; Muñoz-Guerra, S. *J. Polym. Sci., Part A: Polym. Chem.* **1995**, *33*, 299.
(11) Rodríguez-Galán, A.; Bou, J. J.; Muñoz-Guerra, S. *J. Polym. Sci., Polym. Chem. Ed.* **1992**, *30*, 713.
(12) Bou, J. J.; Rodríguez-Galán, A.; Muñoz-Guerra, S. *Macromolecules* **1993**, *26*, 5664.
(13) Bou, J. J.; Iribarren, I.; Muñoz-Guerra, S. *Macromolecules* **1994**, *27*, 5263.
(14) Bou, J. J.; Muñoz-Guerra, S. *Polymer* **1995,** *36*, 181.
(15) Kinoshita, Y. *Makromol. Chem.* **1959**, *33*, 1.
(16) Doak, K.; Campbell, H. N. *J. Polym. Sci.* **1955**, *18*, 213.
(17) Angyal, S. J. In *The Carbohydrates*; Pigman, W., Horton, D., Eds.; Academic: London, 1972; Vol. IA, p 195.
(18) Zabel, V.; Müller-Fahrnow, A.; Hilgenfeld, R.; Saenger, W.; Pfannemüller, B.; Enkelmann, V.; Welte, W. *Chem. Phys. Lipids* **1986**, *39*, 313.
(19) Müller-Fahrnow, A.; Hilgenfeld, R.; Heese, H.; Saenger, W. *Carbohydr. Res.* **1988**, *176*, 165.
(20) Chen, L.; Haraden, B.; Kane, R. W.; Kiely, D. E.; Rowland, R. S. In *Computer Modelling of Carbohydrate Molecules*; French, A. D., Brady, J. W., Eds.; American Chemical Society: Washington, DC, 1990; p 141.
(21) Chen, L.; Kiely, D. L. *Polym. Prepr. (Am. Chem. Soc., Div. Polym. Chem.)* **1993**, *34*, 550.
(22) Campbell-Smith, P. J.; Arnott, S. *Acta Crystallogr., Sect. A* **1978**, *34*, 3.
(23) CERIUS[2] 1.6, Molecular Simulations Inc., Burlington, MA.
(24) Dewar, M. J. S.; Zoebisch, E. G.; Healy, E. F.; Stewart, J. J. P. *J. Am. Chem. Soc.* **1985**, *107*, 3902.
(25) Alemán, C.; Franco, L.; Puiggalí, J. *Macromolecules* **1994**, *27*, 4298.
(26) Alemán, C.; Bella, J. *Biopolymers* **1995**, *35*, 257.
(27) Stewart, J. J. P. MOPAC, *QCPE Bull.* **1983**, *3*, 1.
(28) Bunn, C. W.; Garner, E. V. *Proc. R. Soc. London, Ser. A* **1947**, *189*, 39.
(29) Muñoz-Guerra, S.; Prieto, A.; Montserrat, J. M.; Sekiguchi, H. *J. Mat. Sci.* **1992**, *27*, 89.
(30) Wunderlich, B. *Macromolecular Physics*; Academic: New York, 1973; Vol. 1.
(31) (a) Olson, W. K.; Sussman, J. L. *J. Am. Chem. Soc.* **1982**, *104*, 270. (b) Olson, W. K. *J. Am. Chem. Soc.* **1982**, *104*, 278.
(32) Alemán, C.; Martínez de Ilarduya, A.; Giralt, E.; Muñoz-Guerra, S. submitted.
(33) Cannon, C. G. *Spectrochim. Acta* **1960**, *16*, 302.
(34) Jonhson, C. R. ORTEP Report ORNL-3794; Oak Ridge National Laboratory: Oak Ridge, TN, 1965.
(35) Fraser, R. D. B.; MacRae, T. P. *Conformation in Fibrous Proteins*; Academic: New York, 1973.
(36) Voigt-Martin, I. G.; Garbella, R.; Schumacher, M. *Macromolecules* **1992**, *25*, 961.
(37) Voigt-Martin, I. G.; Simon, P.; Yan, D.; Yakimansky, A.; Bauer S.; Ringsdorf, H. *Macromolecules* **1995**, *28*, 243.

MA951394V